



Contents lists available at ScienceDirect

# Medical Engineering and Physics

journal homepage: [www.elsevier.com/locate/medengphy](http://www.elsevier.com/locate/medengphy)

## Computational optimization of a novel atraumatic catheter for local drug delivery in coronary atherosclerotic plaques

Sunandita Sarker<sup>a,\*</sup>, Yiannis S. Chatzizisis<sup>b</sup>, Benjamin S. Terry<sup>a</sup><sup>a</sup> Terry Research Lab, Department of Mechanical and Materials Engineering, 360 Walter Scott Engineering Center, University of Nebraska, City Campus, W342 NH, Lincoln, NE 68588-0526, USA<sup>b</sup> College of Medicine, University of Nebraska Medical Center, 982265 Nebraska Medical Center, Omaha, NE 68198, USA

### ARTICLE INFO

#### Article history:

Received 12 August 2019  
 Revised 18 December 2019  
 Accepted 10 March 2020  
 Available online xxx

#### Keywords:

Computational fluid dynamics (CFD)  
 Coronary atherosclerosis  
 Local drug delivery  
 Non-Newtonian blood flow  
 Drug delivery catheter

### ABSTRACT

Early identification and treatment of high-risk plaques before they rupture, and precipitate adverse events constitute a major challenge in cardiology today. Computational simulations are a time- and cost-effective way to study the performance, and to optimize a system. The main objective of this work is to optimize the flow of a novel atraumatic local drug delivery catheter for the treatment of coronary atherosclerosis. The mixing and spreading effectiveness of a drug fluid was analyzed utilizing computational fluid dynamics (CFD) in a coronary artery model. The optimum infusion flow of the nanoparticle-carrying drug fluid was found by maximizing the drug volume fraction and minimizing drug velocity at the artery wall, while maintaining acceptable wall shear stress (WSS). Drug velocities between 15 m/s and 20 m/s are optimum for local drug delivery. The resulting parameters from this study will be used to fabricate customized prototypes for future in-vivo experiments.

© 2020 IPPEM. Published by Elsevier Ltd. All rights reserved.

### 1. Introduction

Atherosclerosis is a systemic disease with a local manifestation [1]. Inflammation is a crucial pathobiological feature of high-risk atherosclerotic plaque that promotes plaque progression and disruption [2]. Anti-inflammatory drugs have the potential to stabilize and thereby prevent rupture of atherosclerotic plaque [3]. To date, high-risk plaque therapies have been mostly systemic (e.g., statins) limiting local percutaneous therapies to the treatment of stable, stenosed plaques responsible for the syndrome of stable angina [4]. The concept of local plaque-specific therapy via catheter delivery of anti-atherosclerotic agents (in the form of lipid nanoparticles) to limit the severity of inflammation, stabilize the plaque and thereby avert adverse outcomes is of paramount importance [5]. The clinical and economic implications of identifying and treating high-risk individual lesions before an adverse event can occur are anticipated to be enormous.

Catheters are the foundation of effective local drug delivery. Currently, commercially available drug delivery catheters are The ClearWay RX (Atrium Medical Corporation, Hudson, NH) and Bullfrog (Mercator MedSystems, Inc.) [6,7]. These catheters are designed to deliver drugs locally in small vessels; however, they

make physical contact with the vessel wall, which can induce further complications including rupture of the atherosclerotic plaque that is being treated. Because of this risk and the non-atraumatic nature of the existing catheters, they are mostly used in peripheral arteries. We introduced a novel atraumatic catheter in our previous work to address this problem and validated it on a bench-top setup [8]. The previous study hypothesized that a particular atraumatic catheter with infusion pores injects drugs radially into the blood flow, and the streamlines carry the drug to the low-velocity region near the vessel wall. The concept was validated, and the design parameters were determined in a computational fluid dynamics (CFD) model with a laminar flow of Newtonian fluids and a bench-top experiment. However, for both fluids, blood and drug, only the properties of water were used in the validation and the turbulence effect of mixing was not considered.

Obtaining detailed measurements for physiological flows that interact with devices or affect drug-delivery performance is time-consuming and expensive to measure using animal or other physiologically representative models. Due to the invasive nature and high cost of in vivo models, experimental work optimizing coronary catheters is limited. CFD can bridge this gap by providing detailed flow-related information for performance assessments that can be used to guide catheter development. The objective of the current work is to optimize the flow of an atraumatic local drug delivery catheter by maximizing the drug volume fraction and

\* Corresponding author.

E-mail address: [sunandita.sarker@huskers.unl.edu](mailto:sunandita.sarker@huskers.unl.edu) (S. Sarker).

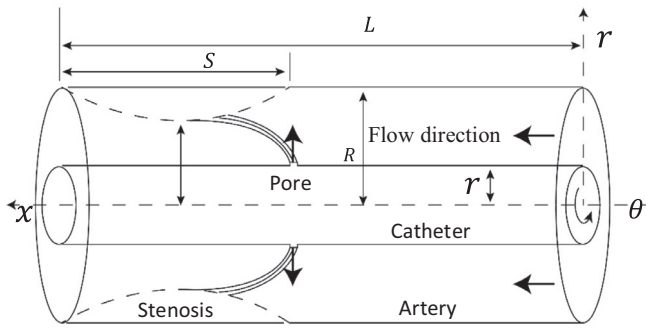


**Fig. 1.** Schematic of the concentric catheter through a stenosed artery, with a no-slip boundary condition in the artery and catheter wall,  $\mathbf{v}(\mathbf{r}, \mathbf{x}, t) = 0$  at  $r = r_0$ ;  $r = R_0$ . Initially, the system was at rest, and the annulus section was filled with only blood ( $\mathbf{v}(\mathbf{r}, \mathbf{x}, 0) = 0$  and  $\alpha_1(0) = 1$ ;  $\alpha_2(0) = 0$ ). At the highest point of stenosis, 40% and 70% stenoses were considered. The catheter has two infusion pores equally distributed in 2D and six in 3D models. A fully developed flow was implemented at the artery inlet, and the pressure gradient was implemented at the outlet. Injection flow was considered in the normal direction of the pores.

minimizing drug velocity at the artery wall for the treatment of coronary atherosclerosis.

## 2. Methods

We use CFD to achieve the objective of this work by analyzing the mixing and spreading effectiveness of drug injection and by validating the concept of an atraumatic local drug delivery catheter in an idealized coronary artery model with non-Newtonian blood flow.

In this section, the model geometry, computational modeling, boundary conditions, and convergence criteria used are presented. The mathematical formulation of the governing equations is also discussed for further insight into the modeling. The streamline velocity, drug volume fraction, and wall shear stress (WSS) were computed for the entire range of injection velocities. The infusion flow rate that maximized the drug volume fraction and minimized drug velocity at the wall while maintaining acceptable WSS was calculated.

### 2.1. Model geometry

The flow field was modeled as co-axial tubes with the artery considered to be the outer tube and the catheter as the inner tube [9]. The dimensions and parameters of the computational domain were based on patient-specific physiological values. A nominal radius of the artery,  $R$  was considered to be 1.5 mm [10]. The reduction in cross-sectional area for stenosis in 2D models was 40% and 70%, and for 3D models was only 70%, which are within the range of the pathology [11]. The catheter radius,  $r$ , must be smaller than the minimum radius of the stenosed artery in order to avoid friction and inflammation even in the presence of acute stenosis. Thus a 3–4 F gauge (outer radius,  $r = 0.5$  mm) was selected for the study. A section of the artery ( $L = 20$  mm) with stenosis length ( $S = 10$  mm) and minimum diameter (1.64 mm) was modeled. Appropriate boundary conditions were applied to the truncation surface. For example, the inlet of the truncation had a fully developed velocity profile with a maximum velocity of  $0.44 \text{ ms}^{-1}$ , and the outlet had a constant pressure of 13.3 kPa based on average physiological velocity and blood pressure of coronary artery [12]. The geometric parameters and boundary conditions are illustrated in Fig. 1. In this work, three 2D models (artery without stenosis and arteries with 40% and 70% stenosis) were analyzed while only two 3D models (arteries with and without stenosis) were analyzed. The 3D stenosed model was created based on a radiograph

**Table 1**  
Mesh Characteristics.

Geometry	No. of nodes	No. of elements
2D without stenosis	20,917	6702
2D with 40% stenosis	66,476	21,499
2D with 70% stenosis	37,385	11,864
3D without stenosis	92,166	232,996
3D with 70% stenosis	1,320,487	952,102

of a real stenosed artery that has approximately 70% stenosis. Two-dimensional models were analyzed first in detail, and then relevant infusion velocities found from 2D analysis were implemented in the 3D models. In the 2D models, the catheter has only two infusion pores at  $180^\circ$  apart, and in the 3D models it had six radially equally distributed pores. All pores in all models were  $20 \mu\text{m}$  in diameter.

### 2.2. Computational modeling

All computational modeling was performed with Fluent 19.2 (Ansys, Inc., Canonsburg, PA, USA). A pressure-based solver was used, and the convergence criterion was specified as  $1e^{-5}$  with the maximum number of iterations set to  $1e^4$  for a steady-state solution. The coupled scheme was adopted for pressure-velocity coupling with default spatial discretization. The realizable  $k-\epsilon$  model was adopted for the turbulent viscosity as the infusion region may have flow features, including strong streamline curvature, vortices, and rotation. For all cases, meshing was performed using Fluent Meshing (Ansys, Inc., Canonsburg, PA, USA). The mesh characteristics are given in Table 1. A mesh independence study was not performed in this work.

The blood was modeled as a single, incompressible, non-Newtonian fluid with a constant density of  $1170 \text{ kg/m}^3$  while the drug was modeled with fluid properties of water. The Carreau viscosity model was used for non-Newtonian blood flow [13]. At low shear rates, fluid in the Carreau model behaves as a Newtonian fluid ( $n = 1$ ), and at high shear, fluid behaves as pseudo-plastic (non-Newtonian,  $n < 1$ ) and as dilatant (non-Newtonian,  $n > 1$ ) fluid. Blood was assumed to have Newtonian behavior for high shear rate flow, such as the flow through larger arteries, and non-Newtonian behavior for low shear rate flow, such as the flow through smaller arteries and downstream of the stenosis [14]. As the Carreau model can be used for both conditions, it is most prevalent in modeling blood flow.

The mathematical modeling of blood flow is accomplished by employing the momentum balance equation and the continuity equation [15]:

$$\rho (\partial \mathbf{v} / \partial t + \mathbf{v} \cdot \nabla \mathbf{v}) = -\nabla p + \nabla \cdot \boldsymbol{\tau} \quad (1)$$

$$\nabla \cdot \mathbf{v} = 0 \quad (2)$$

where  $\mathbf{v}$  is velocity vector,  $p$  is pressure,  $\rho$  is density and  $\boldsymbol{\tau}$  is viscous stress tensor related to the apparent viscosity ( $\mu_a$ ) and shear rate ( $\boldsymbol{\gamma}$ ). Also,

$$\boldsymbol{\tau} = 2\mu_a(\boldsymbol{\gamma})\mathbf{E} \quad (3)$$

$$\boldsymbol{\gamma}^2 = 2\text{tr}\mathbf{E}^2 \quad (4)$$

where  $\mathbf{E}$  is strain rate tensor.

In a simplified 2D form:

$$\mathbf{E} = \begin{bmatrix} \partial u / \partial x & 1/2(\partial u / \partial y + \partial v / \partial x) \\ 1/2(\partial u / \partial y + \partial v / \partial x) & \partial v / \partial y \end{bmatrix}. \quad (5)$$

The apparent viscosity ( $\mu_a$ ) for the Carreau viscosity model is given by the relation:

$$\mu_a = \mu_\infty + (\mu_0 - \mu_\infty) [1 + \lambda^2 \dot{\gamma}^2]^{(n_c - 1)/2} \quad (6)$$

where for human blood,  $\mu_0 = 0.056$  Pa s,  $\mu_\infty = 0.00345$  Pa s (upper and lower limits of the viscosity corresponding to the low and high shear rates),  $\lambda = 3.313$  s (relaxation time constant) and  $n_c = 0.3568$  (power law index). The coefficients are empirically determined [13].

For the multiphase modeling, the Euler-Euler (EE) technique is typically used for modeling small vessels [16]. In this study, the volume of fluid (VOF), an EE model in Fluent, was used for two immiscible fluids where blood was set as the primary phase and the drug fluid as the secondary phase. The implicit formulation was used to discretize the parameters of the VOF, and the cut-off value of the fraction was set to  $10^{-6}$ . The volume fraction of blood ( $\alpha_1$ ) is 1 where no drug fluid is present and is between 0 and 1 elsewhere. The volume fraction of the injected drug fluid ( $\alpha_2$ ) is determined by  $\alpha_2 = 1 - \alpha_1$ . The governing equation for volume fraction is:

$$\partial \alpha_1 / \partial t + \mathbf{v} \cdot \nabla \alpha_1 = \nabla \cdot (\mathbf{V}_f \nabla \alpha_1) \quad (8)$$

where,  $\mathbf{V}_f = D + \mu_t / \rho S_{c_t}$ ,  $\mu_t$  being the turbulence viscosity,  $S_{c_t}$  as the turbulence Schmidt number and  $D$  the mass diffusivity of the drug fluid in the blood. The mixture density is  $\rho = \alpha_1 \rho_1 + \alpha_2 \rho_2$ . Effective viscosity is given by:

$$\mu_e = \mu_t + \mu \quad (9)$$

where  $\mu = \mu_a \rho_1 + \mu_2 \rho_2$ .

A system of equations including (1), (2), and (8) needed to be solved to get the flow field and velocity profile. The no-slip boundary conditions at the artery wall, as well as at the catheter wall, are:

$$\mathbf{v}(\mathbf{r}, \mathbf{x}, \mathbf{t}) = 0 \text{ at } r = r_0 ; r = R_0 \quad (10)$$

where  $r_0$  and  $R_0$  are, respectively, the radii of the catheter and artery.

It is further assumed that initially the system is at rest, and the domain has been occupied with only blood. That means:

$$\mathbf{v}(\mathbf{r}, \mathbf{x}, 0) = 0 \quad (11)$$

$$\alpha_1(0) = 1; \alpha_2(0) = 0. \quad (12)$$

Assumptions were made to simplify the complexity of the flow dynamics of an actual stenosed artery with drug fluid and blood mixing. The blood was modeled as a single-phase incompressible fluid, ignoring the presence of the various blood components, including different types of blood cells and plasma. The effect of nanoparticles on the drug fluid was ignored. Also, an assumption was made that the nanoparticles follow the drug streamlines, and upon arriving at the arterial wall are absorbed into the inflamed tissue. Simulating particle uptake was beyond the scope of this study. The transient behavior of the blood and drug fluid interaction near the injection pores and arterial wall where the effects of mixing are most relevant were well accounted for. The rigid wall assumption was made with a no-slip boundary condition for both catheter and artery walls. The increase in pressure due to catheter insertion was neglected. Frictional resistance on the curved surface of the catheter was also neglected. Other work has shown that the geometry of stenoses is time-variant [15,17], but our period of interest was so short that this could be neglected. Although a highly unsteady flow field is present with pulsatile blood flow and viscoelastic artery walls [18], the models generated in this study were considered to be at steady-state flow because the period of interest was minimal compared to a cardiac cycle.

### 2.3. Analysis of results

The optimal infusion flow of the nanoparticle-carrying drug fluid was found by maximizing the drug volume fraction and minimizing drug velocity at the artery wall, while maintaining acceptable WSS. A fully developed parabolic radial velocity profile was applied at the inlet of the artery. The velocity of the blood flow started decreasing almost linearly when the radial distance was less than 0.2 mm from the wall; therefore, this region was considered low-velocity. If the injection velocity is too low, nanoparticles are washed away by the axial blood flow before reaching the artery wall. Five different radial injection velocities were selected (5 m/s, 10 m/s, 15 m/s, 20 m/s, and 25 m/s). The resulting Reynolds numbers for injecting drug fluid were 112, 225, 337, 449, and 562, respectively. Injection streamlines were exported to evaluate minimum velocity sufficient for the streamlines to reach the low-velocity region so that nanoparticles get maximum contact for absorption by the inflamed artery wall.

To assess the mixing efficiency at different injection velocities, the contour of drug volume fraction,  $\alpha_2$ , was plotted against the 2D artery geometries. The values of the contours ranged from 0, only blood (blue) to 1, only drug fluid (red) with intermediary values representing the mixture of the two fluids. All measurements were taken in the same 2D computational symmetry plane. Also, the volume fraction of the drug ( $\alpha_2$ ) along the axial length from the infusion plane was exported to evaluate the injection velocity for the maximum volume fraction of the drug.

For 3D geometries, the flux of drug through a 0.2 mm thick annular regions (low-velocity region) spaced every 1 mm from the infusion plane was calculated along with the total flow through each cross-section. The percentage flow through the annulus region was used to compare performance.

Endothelial cells can undergo significant injury from a WSS larger than 38 Pa [19]. Therefore, it is necessary to have the WSS within this range for the optimal flow. To assess the effect of injection velocity on WSS, contours of WSS at the 3D artery wall were analyzed for the specified injection velocities. All of the results from each model were generated using ANSYS CFD-post for comparison.

## 3. Results

### 3.1. Streamline velocity

For the 2D model without stenosis, only streamlines for 15 m/s, 20 m/s, and 25 m/s reached the low-velocity region described in the methods section. The average velocities of the streamlines in the low-velocity region are 3.27 m/s, 4.45 m/s and 5.49 m/s for 15 m/s, 20 m/s, and 25 m/s, respectively. Infusion streamlines were simulated for two different stenosed arteries. Only streamlines with 5 m/s infusion velocity did not reach the near-wall low-velocity region (0.2 mm near the lesion wall) in both geometries. For the 70% stenosed artery, the average velocities of the streamlines in the low-velocity region were 2.29 m/s, 3.59 m/s, 4.60 m/s, and 5.91 m/s for 10 m/s–25 m/s infusion velocities, while for the 40% stenosed artery they were 1.91 m/s, 3.27 m/s, 4.58 m/s, and 5.58 m/s.

In the 3D model, infusion with velocities 15 m/s, 20 m/s, and 25 m/s were simulated inside the artery, starting from all six infusion pores. Only streamlines for 20 m/s, and 25 m/s reached the artery wall and spread, while streamlines for 15 m/s reached the region but did not hit the artery wall. The velocity along the streamline decreased rapidly due to the axial flow of blood and reached a constant value of 0.27 m/s for all cases.

The 3D streamlines starting from all six infusion pores were simulated inside the stenosed artery. Streamlines for 20 m/s and

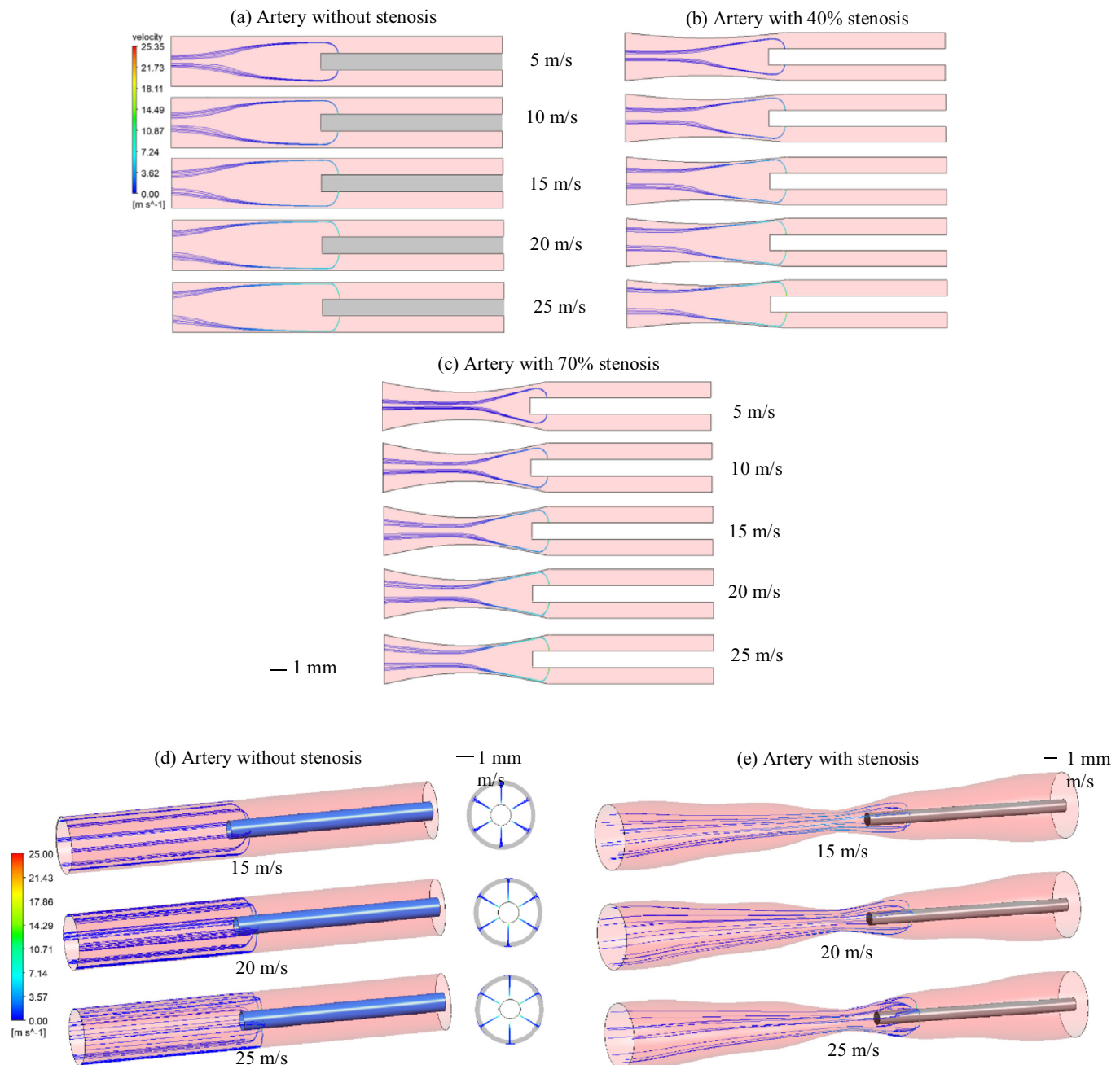


**Fig. 2.** Streamlines starting from infusion pores are plotted for different infusion rates for the 2D (a, b, c) and 3D (d, e) models. The color-map represents the velocity along the streamlines. Streamlines for 20 m/s and 25 m/s reached the artery wall and spread on the wall for all cases.

25 m/s hit the artery wall, while streamlines for 15 m/s only reached the near-wall low-velocity region. An increase in the streamline velocities near the highest stenosed cross-section was observed in all three cases. In Fig. 2, streamlines starting from infusion pores are plotted for different infusion rates for the 3D models. The color-map represents the velocity along the streamlines.

### 3.2. Drug volume fraction

To compare the mixing efficiency of the catheter at different injection velocities, the contour of drug volume fraction,  $\alpha_2$  is plotted against the 2D artery geometry without stenosis. Values of  $\alpha_2$  in the near-wall low-velocity region were within 10%, 40%, 60%, and 70% with velocities for 10, 15, 20, and 25 m/s, respectively. For the larger two infusion velocities, turbulence was observed where

the stream hit the wall, and as a result, drug fluid also spread upstream of the infusion point. In the presence of stenosis, the distance between the artery wall and the infusion pores is small. As a result, larger values of  $\alpha_2$  were noticed in the near-wall low-velocity region. The effects are shown in Fig. 3. For infusion velocities 10 m/s and 15 m/s,  $\alpha_2$  were up to 50% and 60%, respectively, while for both 20 m/s and 25 m/s, the highest  $\alpha_2$  were within 70%. Because of the flow separation effect at the highest stenosed cross-section,  $\alpha_2$  values started to decrease.

Fig. 4 illustrates the spreading of drug fluid along the blood vessel wall. As expected, with an increasing injection velocity, an increase in drug volume fraction was observed. No drug reached the wall with infusion velocities of 5 m/s and 10 m/s. Notably, the increase in drug volume fraction between 15 m/s and 20 m/s was approximately 50% greater than the increase between

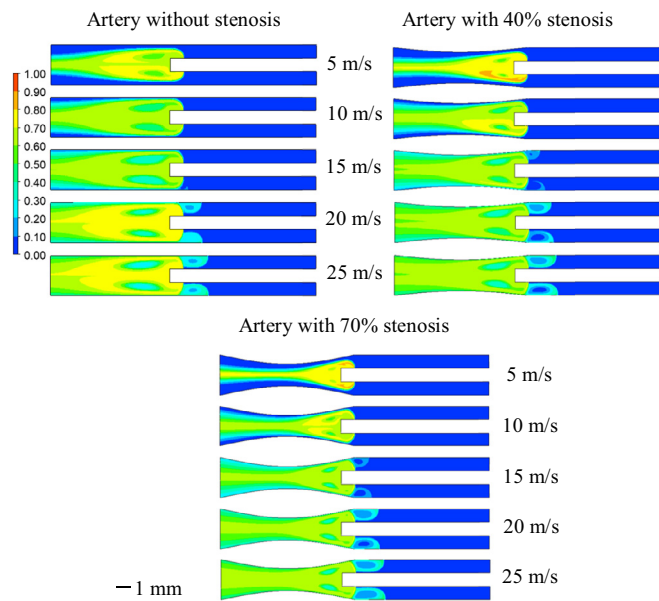


**Fig. 3.** Contours of drug fluid volume fraction at different injection velocities for arteries without stenosis, and with 70% and 40% stenosis. The value of  $\alpha_2$  drops significantly after 5 mm from the infusion plane due to flow separation for arteries with stenosis.

20 m/s and 25 m/s. A similar pattern was observed for stenosed arteries.

To compare the mixing efficiency near the wall for 3D models at different injection velocities, the percentage of the drug flowing through the annulus region near the wall was plotted against the length of the artery (Fig. 5). As expected, with an increasing injection velocity, an increase in volume fraction was observed. However, the difference in the increase of volume fraction between 15 m/s and 20 m/s was markedly larger than the increase in volume fraction between 20 m/s and 25 m/s.

For 3D stenosed arteries, as before, the volume fractions for 20 m/s and 25 m/s infusion velocity were larger than that for 15 m/s. The volume fractions for 20 m/s and 25 m/s infusion velocities were almost identical, indicating that no further improvement in volume fraction may be achieved by increasing the infusion velocity.

### 3.3. Wall shear stress

As expected, WSS increased with an increasing infusion velocity (Fig. 6). An increase was observed where the drug streamline hit the wall. The highest observed WSS for 15 m/s, 20 m/s, and 25 m/s infusion rate are 4.78 Pa, 25.97 Pa, and 36.88 Pa, respectively. The largest WSS was observed within 0.5 mm of infusion. The high WSS region is diminished after 1 mm. Similar to an artery without stenosis, for a stenosed artery, WSS increased with increasing velocity. However, the highest WSS was found at the largest stenosed cross-section, with the values of 28.4 Pa, 36.5 Pa, and 40.451 Pa for 15 m/s, 20 m/s, and 25 m/s infusion rate respectively.

## 4. Discussion

In this work, we designed and optimized an atraumatic drug delivery catheter for coronary atherosclerosis. We observed the mixing and spreading effectiveness for optimizing the flow of an atraumatic local drug delivery catheter for the treatment of coronary atherosclerosis. We employed an incompressible, 2D and 3D, multi-fluid, non-Newtonian, and steady-state numerical formulation that accounts for turbulence effect. The results of our sim-

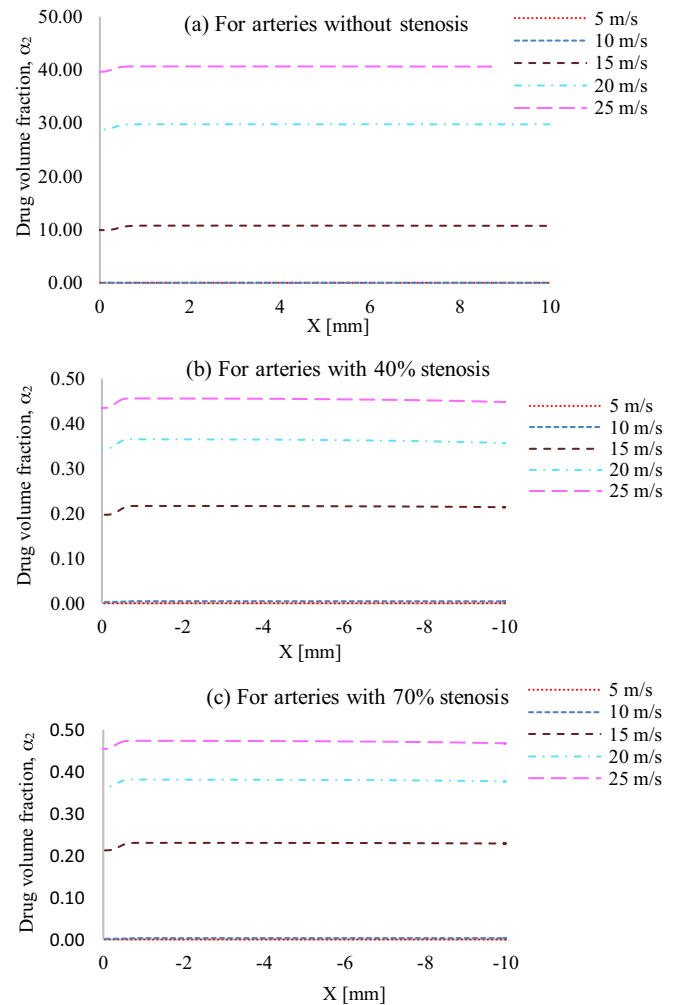


**Fig. 4.** Drug volume fractions,  $\alpha_2$ , plotted versus axial length along the artery wall at different injection velocities. The drug is injected at  $x = 0$  mm. In all cases, an increase in  $\alpha_2$  between 15 m/s and 20 m/s is almost double than between 20 m/s and 25 m/s. Also,  $\alpha_2$  values are larger for the stenosed artery.

ulations provided a detailed characterization of the dynamics of the interaction between the injected drug fluid and the blood flow. This greater detail allows us to optimize the flow that maximizes the drug volume fraction and minimizes drug velocity at the wall while maintaining acceptable WSS.

The streamline velocity near the wall is directly related to the infusion or injection velocity. Streamlines with 15 m/s or above reached the near-wall low-velocity region. The drug volume fraction near and on the wall also increased with infusion velocity. These results suggest that higher infusion flow is preferable for drug delivery on the wall. However, we observed a considerable difference in drug volume fraction between 15 m/s and 20 m/s, but only a slight difference between 20 m/s and 25 m/s. For the stenosed artery, the drug volume fraction was almost identical for 20 m/s and 25 m/s. The WSS increased significantly, with all increases in velocity. With a 25 m/s infusion velocity, WSS was over the critical range for the stenosed artery. A high risk of platelet aggregation and coagulation are associated with high shear exposure. Taken together, the data indicate velocities between 15 m/s and 20 m/s are optimal for local drug delivery. Excessive flow rate from the catheter infusion pore may damage the blood vessel and blood cells. Damage might be substantial when the shear forces on the wall are presented for nearly one hour or more [19]. A typical infusion will last for less than 5 min, so this risk is reduced,

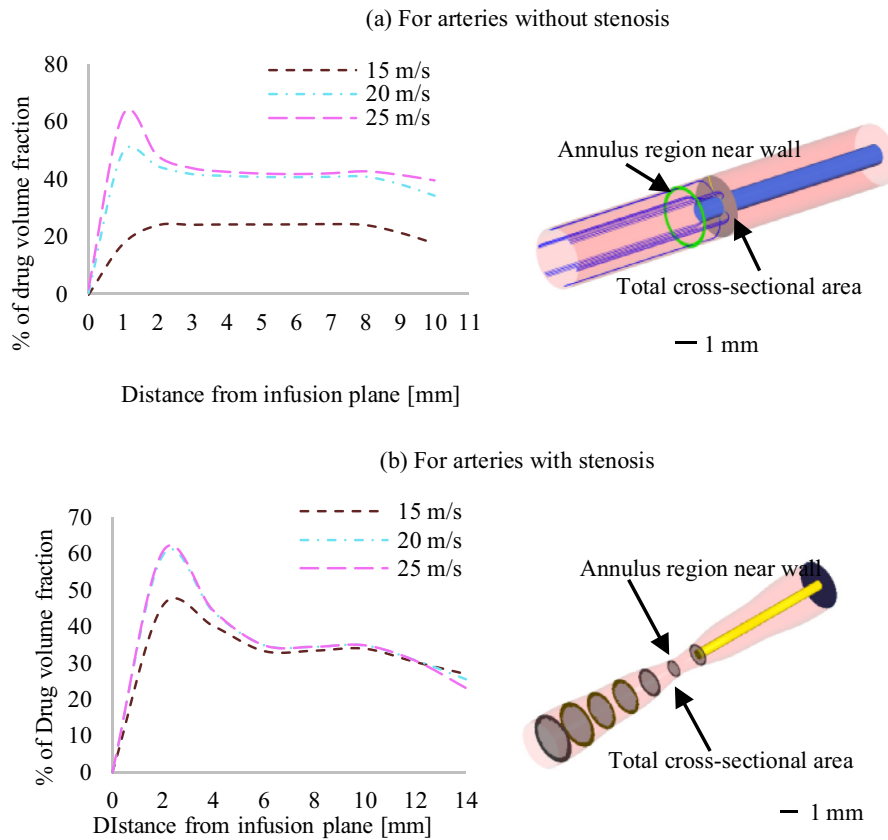


**Fig. 5.** Percentage of drug fluid volume fraction at different injection velocities at different distances from the infusion plane. With an increasing injection velocity, an increase in volume fraction was observed. There is a larger difference between 15 m/s and 20 m/s compared to the difference between 20 m/s and 25 m/s, with almost identical trends for stenosed arteries.

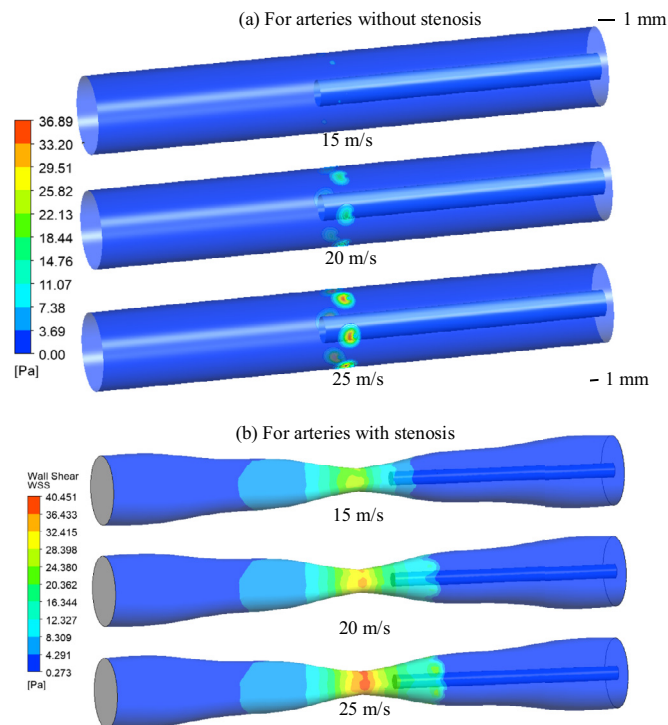


**Fig. 6.** Contours of WSS at different injection velocities, 15 m/s, 20 m/s, and 25 m/s, on the artery wall. The drug was injected at  $x = 10$  mm. The effect on WSS was present before drug injection because of turbulence. The peak of WSS was observed within 0.5 mm of infusion in the artery without stenosis, and regular WSS was achieved after 1 mm (Fig. 6a). The highest WSS was found at the largest stenosed cross-section, rather than where the streamline hit the wall.

although not eliminated. Future in vitro and in vivo studies are essential to entirely optimize the infusion flow properties.

The current study has several limitations. Catheters were compared at steady-state blood flow and although our timescale merits the steady-state assumption, there may be some differences in flow behavior with pulsatile flow. A time-dependent injection profile with the capability of reducing high concentration effects deserves investigation. It should be noted that pulsatile flow also impacts the viscoelasticity and time-variant cross-section of the vessel wall, resulting in changes in blood flow. These effects certainly deserve special attention along with the changing nominal diameter in the axial direction, and further branching. Due to branching of coronary arteries, the velocity profile of blood might not be fully developed at the inlet. Moreover, blood pressure changes with pulse, but in our study the outlet pressure was held constant and flow separation of each case was also not analyzed. As shown by Clark et al. in [20], flow separation could have thrombogenic effects, which warrants further investigation in the context of our model. Although computational work on catheter delivery is limited, our results match with an existing related study. As shown by Asrara and Aldredge [18], modified catheters with side holes exhibit good spreading and mixing properties. Their study also showed that the spreading effectiveness of a catheter is determined by the flow rate of the injected fluid and is greatest at large flow rates. They also correlated spreading and injection flow of the drug to the viscosity of the injected fluid which was not analyzed in our current study.

**5. Conclusion**

Nowadays, CFD is an established and well-defined approach for building and testing complex representations of the cardiovascular

system, enhancing diagnostic assessment, assisting device design and clinical trials [21]. Accurately quantifying flow effects around cardiovascular devices in-vivo is very complicated, expensive and in some cases impossible. CFD is well suited to quantify such internal flow conditions, as was shown in our current study. In context of device development, the relationship between design parameters and flow characteristics can be analyzed using CFD to reduce the number of design iteration. For example, CFD has proven to be an excellent tool for stent design [22] and has been very beneficial in the development of this catheter. CFD models are easily reproducible and can be used to discover and validate performance in patient-specific geometries. As a result, performance of a newly developed catheter can be analyzed before clinical practice. The benefits of CFD are recognized by regulatory authorities and standardized methods for validating CFD simulations are being considered [23]. In this work, we analyzed the mixing and spreading effectiveness of the drug delivery catheter utilizing CFD. A series of simulations with increasing complexity were performed using a commercial CFD tool to develop this catheter and optimize relevant parameters.

In contrast to the currently available drug delivery catheters, our novel catheter does not make physical contact with the plaque and is capable of infusing drugs locally in a stenosed coronary artery. The catheter model was implemented on an idealized non-Newtonian stenosed arterial blood flow model without pulsatile flow. The results of the simulation indicate that administering drugs between 15 m/s and 20 m/s infusion velocity to the stenosed wall is effective and within safe levels of WSS. With a higher infusion velocity, the drug volume fraction near the wall increased, but the drug fluid injected through the infusion pores at a high injection velocity may cause damage due to WSS. The resulting parameters from this study will be used to fabricate customized prototypes for future in-vivo experiments. Properties of this prototype catheter include a hydrophilic coating, soft shaft, flexible distal segment, and dual lumen for guidewire use, enabling advancement and access through tortuous distal vessels.

### Declaration of Competing Interest

None.

### Funding

This work was supported by UNL and UNMC Sciences, Engineering and Medicine Initiative funds.

### Ethical Approval

Not required.

### References

- [1] Chatzizisis YS, Coskun AU, Jonas M, Edelman ER, Feldman CL, Stone PH. Role of endothelial shear stress in the natural history of coronary atherosclerosis and vascular remodeling: molecular, cellular, and vascular behavior. *J Am Coll Cardiol* 2007;49:2379–93. doi:10.1016/j.jacc.2007.02.059.
- [2] Virmani R, Kolodgie FD, Burke AP, Farb A, Schwartz SM. Lessons from sudden coronary death. *Arterioscler Thromb Vasc Biol* 2000;20:1262–75. doi:10.1161/01.ATV.20.5.1262.
- [3] Bäck M, Hansson GK. Anti-inflammatory therapies for atherosclerosis. *Nat Rev Cardiol* 2015;12:199–211. doi:10.1038/nrcardio.2015.5.
- [4] Weber C, Noels H. Atherosclerosis: current pathogenesis and therapeutic options. *Nat Med* 2011;17:1410–22. doi:10.1038/nm.2538.
- [5] Lobatto ME, Fuster V, Fayad ZA, Mulder WJM. Perspectives and opportunities for nanomedicine in the management of atherosclerosis. *Nat Rev Drug Discov* 2011;10:835–52. doi:10.1038/nrd3578.
- [6] Saraf S, Ong P, Gorog D. ClearWay™ rx - Rapid exchange therapeutic perfusion catheter. *EuroIntervention* 2008;3:639–42. doi:10.4244/EIJV3I5A114.
- [7] Owens CD, Gasper WJ, Walker JP, Alley HF, Conte MS, Grenon SM. Safety and feasibility of adjunctive dexamethasone infusion into the adventitia of the femoropopliteal artery following endovascular revascularization. *J Vasc Surg* 2014;59:1016–24. doi:10.1016/j.jvs.2013.10.051.
- [8] Sarker S, Chatzizisis YS, Kidambi S, Terry BS. Design and development of a novel drug delivery catheter for atherosclerosis. In: *Proceedings of the Design of Medical Devices Conference*; 2018. <https://doi.org/10.1115/DMD2018-6869>.
- [9] Srivastava VP, Rastogi R. Blood flow through a stenosed catheterized artery: effects of hematocrit and stenosis shape. *Comput Math Appl* 2010;59:1377–85. doi:10.1016/j.camwa.2009.12.007.
- [10] Dodge JT, Brown BG, Bolson EL, Dodge HT. Lumen diameter of normal human coronary arteries. Influence of age, sex, anatomic variation, and left ventricular hypertrophy or dilation. *Circulation* 1992;86:232–46. doi:10.1161/01.CIR.86.1.232.
- [11] Choi G, Lee JM, Kim H-J, Park J-B, Sankaran S, Otake H, et al. Coronary artery axial plaque stress and its relationship with lesion geometry: application of computational fluid dynamics to coronary CT angiography. *JACC Cardiovasc Imaging* 2015;8:1156–66. doi:10.1016/j.jcmg.2015.04.024.
- [12] Dole WP, Richards KL, Hartley CJ, Alexander GM, Campbell AB, Bishop VS. Diastolic coronary artery pressure-flow velocity relationships in conscious man. *Cardiovasc Res* 1984;18:548–54. doi:10.1093/cvr/18.9.548.
- [13] Shibeshi SS, Collins WE. The rheology of blood flow in a branched arterial system. *Appl Rheol Lappersd Ger Online* 2005;15:398–405. doi:10.1901/jaba.2005.15-398.
- [14] Akbar NS, Nadeem S. Carreau fluid model for blood flow through a tapered artery with a stenosis. *Ain Shams Eng J* 2014;5:1307–16. doi:10.1016/j.asej.2014.05.010.
- [15] Jian T.C., Amin N. Analysis of blood flow through a catheterized stenosed artery using mathematica, Johor Bahru, Malaysia: 2016, p. 030048. doi:10.1063/1.4954584.
- [16] Huang J, Lyczkowski RW, Gidaspow D. Pulsatile flow in a coronary artery using multiphase kinetic theory. *J Biomech* 2009;42:743–54. doi:10.1016/j.jbiomech.2009.01.038.
- [17] Mandal PK. An unsteady analysis of non-Newtonian blood flow through tapered arteries with a stenosis. *Int J Non Linear Mech* 2005;40:151–64. doi:10.1016/j.ijnonlinmec.2004.07.007.
- [18] Ararsa K, Aldredge RC. Computational analysis of catheter-tip geometries for optimizing drug infusion in arterial blood flow. *Am J Biomed Eng* 2013;3:91–8.
- [19] Piper R, Carr PJ, Kelsey LJ, Bulmer AC, Keogh S, Doyle BJ. The mechanistic causes of peripheral intravenous catheter failure based on a parametric computational study. *Sci Rep* 2018;8:3441. doi:10.1038/s41598-018-21617-1.
- [20] Clark TWI, Isu G, Gallo D, Verdonck P, Morbiducci U. Comparison of symmetric hemodialysis catheters using computational fluid dynamics. *J Vasc Interv Radiol* 2015;26:252–259.e2. doi:10.1016/j.jvir.2014.11.004.
- [21] Morris PD, Narracott A, Tengg-Kobligk Hvon, Soto DAS, Hsiao S, Lungu A, et al. Computational fluid dynamics modelling in cardiovascular medicine. *Heart* 2016;102:18–28. doi:10.1136/heartjnl-2015-308044.
- [22] Frank AO, Walsh PW, Moore JE. Computational fluid dynamics and stent design. *Artif Organs* 2002;26:614–21. doi:10.1046/j.1525-1594.2002.07084.x.
- [23] Malinauskas RA, Hariharan P, Day SW, Herbertson LH, Buesen M, Steinseifer U, et al. FDA benchmark medical device flow models for CFD validation. *ASAIO J* 2017;63:150. doi:10.1097/MAT.0000000000000499.